THE RESISTANCE SWITCHING PROPERTIES AND MECHANISM IN Ag /ZrO$_2$/Ta SANDWICH STRUCTURE

Y. YUAN[a,*], J. SU[b], H. REN[a], X. LI[b], J. LI[b], W. CHEN[a]
*aDept. of Electronic Engineering, Center for Intelligent Medical Electronics,
Fudan University, 200433, Shanghai,China*
*bDept. of Optical Science and Engineering, Fudan University, 200433, Shanghai
China*

The resistive memory device based on Ag/ZrO$_2$/Ta structure was prepared by using the magnetron sputtering technique. The field emission scanning electron microscopy (FESEM) was applied to investigate the microstructure of device. The Raman spectra was obtained to characterize the ZrO$_2$ structure. The measurement result of current-voltage (*I-V*) shows that the fabricated device exhibits stable bipolar resistive switching (RS) characteristics under room temperature. The underlying mechanism of resistive switching can be correlated with the trap-filled space-charge limited conduction (SCLC) and the trap distribution. The SET and RESET operation voltages shows little change distribution during repeated operations. The characteristics retention exhibits excellent. The achieved characteristics of the RS based on amorphous ZrO$_2$ show as a promising candidate for nonvolatile memory applications.

1. Introduction

Memristor as the the fourth fundamental passive circuit element was proposed by Leon Chua in 1971[1], which is regarded as a promising solution to the problem of traditional semiconductor technologies facing the physical and economical limits[2, 3]. Resistive random access memory (RRAM) is a typical application in the memristor family which is based on the resistance switching characteristics changing a low resistance state (LRS) between and a high resistance state (HRS) by current or voltage stimulus[4]. RRAM has been attracted extensive research attention and intensively studied not only due to its simple structure, excellent scalability, high-speed operations, low power consumption, high endurance, and high density integration [5-8], but duo to its widely potential application for the next-generation nonvolatile memory [9], logic operation [10, 11], neuromorphic circuits [12-14], programmable analog circuits [15, 16]. The RS behaviors have been confirmed to exist in various materials such as transition metal oxide [17], perovskite oxides [18], chalcogenides [19, 20], carbon nanotube[21], organic materials [22], ferroelectric materials [23, 24] and even some graphene-based structures [25].

The transition metal oxide ZrO$_2$ as one of the most promising potential candidates for SiO$_2$ has been reported for owing to obvious RS characteristics [26-30]. Meanwhile, its RS mechanisms have been extensively discussed, mainly including ionic migration and pure electronic effect theory [31]. However, the RS mechanisms may be more complex, which is probably a combination effect with the ionic effect, electronic effect, and even the thermal effect. Realizing the RS underlying mechanism is a key important for controlling the RS device accurately, which is beneficial for the development and application of RRAM. The amorphous ZrO$_2$ film owing high dielectrics in advanced semiconductor [32]. Compared with the polycrystalline films, the current leakage in amorphous oxide films can be effectively depressed by eliminating or reducing leaking paths associated with the grain boundaries [33]. In the literature, much research attention has been paid to the ReRAM applications of crystalline ZrO$_2$ films. However, the research on amorphous ZrO$_2$ is rare, so it is useful and essential to study the

---

* Corresponding author: yyf@fudan.edu.cn

RS based on amorphous ZrO_2 and investigate its RS underlying mechanism of conduction.

In this work, the device $Ag/ZrO_2/Ta$ with metal-insulator-metal (MIM) structures was fabricated by using the magnetron sputtering technique. The RS characteristics parameters and reliability was examined by *I-V* measurements. Then the intrinsic RS underlying mechanism was investigated.

2. Experimental

The device in this study was fabricated by using a radio frequency (RF) magnetron sputtering method under the room temperature. The chamber was evacuated down to approximately 8×10^{-6} mbar. The working pressure is approximately 3.4×10^{-3} mbar with Ar at the flow of 70 SCCM. The bottom electrode (BE) of W was deposited about 50 nm thickness on SiO_2/Si (100) substrates. As a function layer, then the 200 nm thickness ZrO_2 film was deposited. To achieve the metal-insulator-metal (MIM) sandwiched structure, the Ag top electrode (TE) with about 80 nm was deposited on the structure. The Raman spectra was recorded by Raman micro-spectroscopy. The field emission scan electron microscopy (FESEM) was applied to characterize the device microstructure. And, the device electrical characteristics were carried out by the semiconductor parameter analyzer (Agilent B2912A) at room temperature

3. Results and discussion

The cross sectional SEM image of the Ag/ ZrO_2/Ta device, as shown in the Fig. 1(a), reveals that the function layer is about 200 nm thickness with apparently sandwiched structure. The BE and TE layers are about 50 nm and 80 nm thickness, respectively. The thickness of SiO_2 layer is round 350 nm. To identify the structure, the Raman spectra of the film was collected and shown in Fig. 1(b). The energy range of vibrations for the sample extends to around 500 cm^{-1}. The Raman peak at 182 cm^{-1}, 199 cm^{-1}, 320 cm^{-1}, 380 cm^{-1} and 475 cm^{-1} is correlated to ZrO_2 which is coincident with other work [34].

a)   *b)*
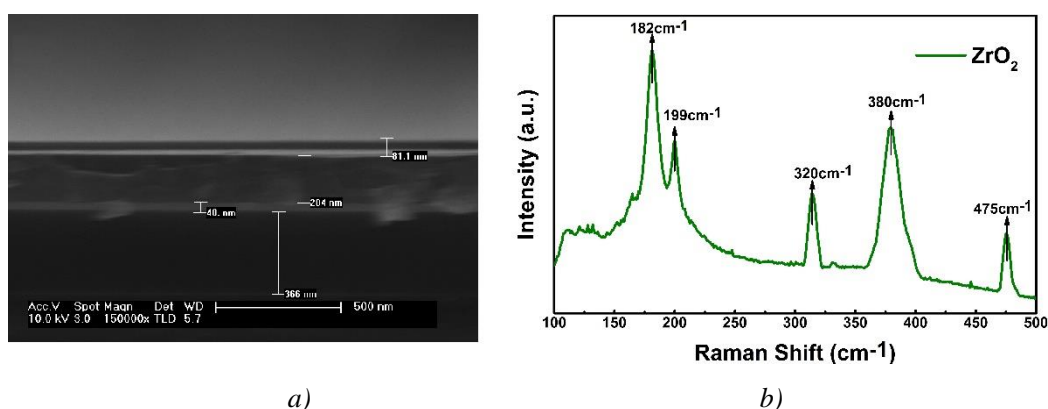
Fig. 1. (a). The cross sectional SEM image of the Ag/ ZrO_2/Ta device. (b) The Raman spectra of ZrO_2 film.

The typical *I-V* characteristics of $Ag/ZrO_2/Ta$ RS device was shown in Fig. 2(a) with a current compliance of 100 mA. The sweep arrow indicates the sweeping directions. The measurement sweep operation voltage was scanned with 0 V→2.5 V→0 V→-2.5 V→0 V. It was obviously shown that the fabricated exhibited bipolar resistive switching behavior. The device was shifted from HRS to LRS during the positive bias sweep voltage which known as the SET process. Then, the device returns into to HRS during the negative bias sweep voltage which is known as the RESET process.
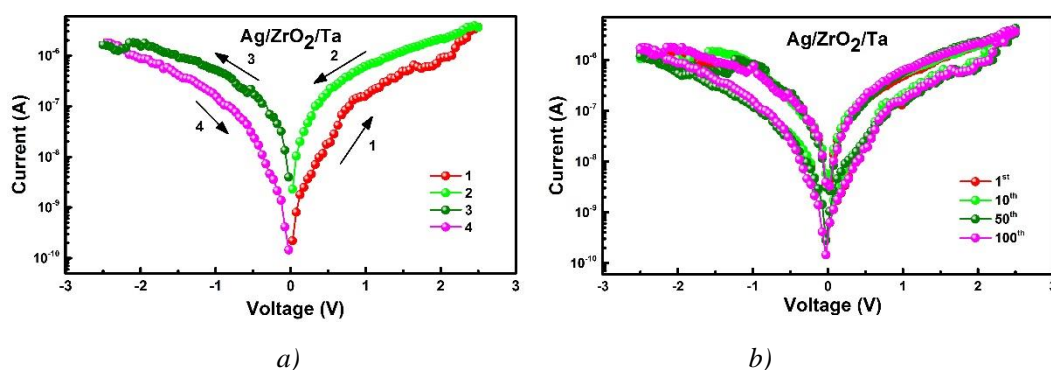
Fig. 2. (a). Typical bipolar I-V characteristic of Ag/ZrO$_2$/Ta in sweeping DC Voltages. (b). The I-V characteristic of Ag/ZrO$_2$/Ta for a certain times cycles.

It is clear that the threshold voltages were approximately 1.8 V (SET) and -1.5 V (RESET), respectively. The difference in the value of SET and RESET voltage may be related to asymmetric electrode. The Ag was used as an active electrode, while the Ta was used as an inert electrode. The device RS behavior based on Ag/ZrO$_2$/Ta exhibits stable bipolar RS characteristics was shown in Fig 2(b).during the 100 cycles loop subsequent voltage sweeping process from 2.5 to -2.5 V. Several conduction mechanism models[2, 12, 35] have been developed to interpret the RS non-liner *I-V* characteristics, such as Schottky emission ($\ln I \propto V^{1/2}$), Poole-Frenkel emission ($\ln I/V \propto V^{1/2}$), Flower-Nordheim tunneling ($\ln I/V^2 \propto V^{-1}$) and space-charge limited conduction (SCLC) ($I \propto V^2$). The device RS characteristics may be related with several conduction mechanisms at the same time. So the method to distinguish these different conduction mechanisms is essential and important.

To further investigate the RS mechanism in the Ag/ZrO$_2$/Ta device, the replotting *I-V* curves in double logarithmic plots was displayed in Fig. 3. The SCLC mechanism can best interpret the RS features during the HRS within positive bias region. The similar phenomenon also was observed in other studies [26, 28, 29]. The device slope within the low bias region is very close to linear due to the Ohmic law region ($I \propto V$). Over the SET operation voltage (1.8 V) sweeping, the current follows square dependence on voltage which may be corresponding to the Child's square law region ($I \propto V^2$). The Current density under the trap-filled SCLC can be expressed by following equations [36]:

$$J = \left(\frac{\theta}{\theta + 1}\right)\frac{9\mu\varepsilon_r\varepsilon_0 V^2}{8L^3}$$

Where, J is the current density; N_c is the effective density states in conductive band, N_t is the emptied electron traps number, $\theta = (N_c/N_t)e^{-(E_c-E_t)/kT}$ is the ratio for free electron and trapped electron, k is the Boltzmann constant,ε_0 is the permittivity of frees pace, ε_r is the static dielectric constant, V is the applied voltage, μ is the electron mobility and L is the thickness of film.

During the low sweeping voltage region, The device *I-V* characteristic is dominated by Ohmic mechanism due to that the thermally generated free electrons density inside the device is greater than the injected electrons from electrode when majority of electron traps are emptied ($\theta \ll 1$). The Ohmic mode happens under electrically quasi neutral state when the partial trap centers were filled during weak injection. In this condition, the current density can be rewritten as following:

$$J = \theta\frac{9\mu\varepsilon_r\varepsilon_0 V^2}{8L^3}$$

In the of strong injections process, the increase of applied voltage may increase the density of free carriers resulting from injection to such a value that the Fermi level moves up above the electron trapping level. Then, the majority of electron traps are occupied ($\theta \gg 1$), which means the density of injected electrons gradually exceeds the thermal equilibrium concentration in the cell. The cell *I-V* characteristics are dominated by the injected electrons and the *I-V* relationship is corresponding to the square law. In this case, the current density equation can be rewritten as

follows:

$$J = \frac{9\mu\varepsilon_r\varepsilon_0 V^2}{8L^3}$$

During the positive voltage sweeping, It was observed that the *I-V* slop changes from ~2 to ~4.3 which may be correlated with the traps density distribution. The traps density distribution can be expressed by following equation [19]:

$$D(E) = \frac{N_t}{kT_c} exp\left(-\frac{E - E_v}{kT_c}\right)$$

Where, $D(E)$ is the traps density per unit energy range above the valance band edge, T_c is the characteristic temperature, N_t is the total density of traps, k is the Boltzmann constant and N_t/kT_c is the traps at the valence band edge.
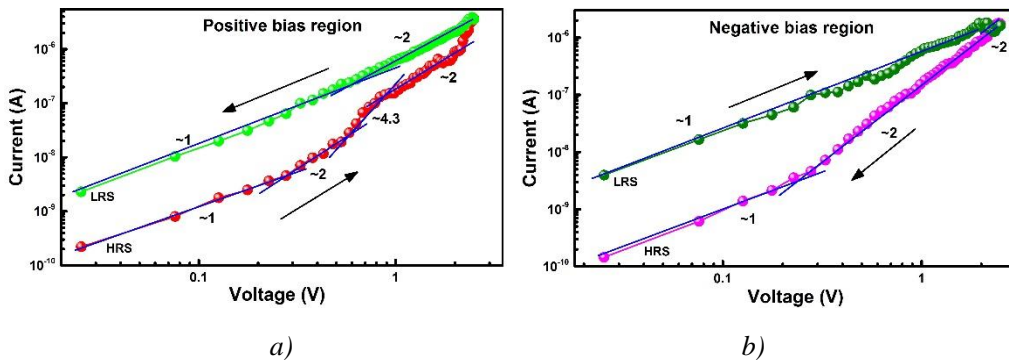
Fig. 3. (a). Positive bias region in logarithmic plot. (b). Negative bias region in logarithmic plot.

Generally, the many defects in the polycrystalline can mainly be divided two types: (i) the defects within grain boundaries arising from dangling bonds, (ii) the defects within crystalline grain [35]. The processing of defects forming localized states near the valance band can be regarded as charge traps and absorb injected carriers [37]. The RS state is dependent on the carrier trapped levels. The high trapped level is corresponding to the device LRS and the low trapped level is corresponding to the device HRS. The device resistance turns into LRS when all the deep traps are filled.

During the negative voltage sweeping with 0 V→−2. 5V, It is noted that the *I-V* slop can be best fitted with Ohmic law, as shown in Fig 3(b). In this case, the device RS mechanism may be due to the Ag filament formation. The similar RS mechanism was observed in other works [27, 30]. The Ag filament formation process can be described as follows:

$$Ag \rightarrow Ag^+ + e$$
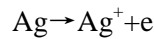
The Ag atoms are oxidized to Ag ions as described above When the Ag electrode is stimulated with the positive voltage sweeping.

$$Ag^+ + e \rightarrow Ag$$
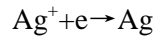
These Ag ions will migrate toward the Ta electrode and they are reduced back to metallic Ag atoms as described above when the applied electric field is increasing strong on the device. When the sweeping voltage reaches SET voltage, the formed metallic Ag filament finally reaches the Ag electrode. Meanwhile, the device resistance drops abruptly turning into LRS. In this condition, the device current density duo to Ohmic conduction can be expressed by following equation [35]:

$$J = \sigma E = \frac{nq\mu V}{L}$$

Where σ is the electrical conductivity, μ is the electron mobility, n is the number of

electrons, V is the stimulated voltage. During the negative voltage sweeping region, the device resistance turns from LRS to HRS state which was occurred at the -1.5 V RESET voltage. The formed Ag filament was ruptured by Joule heat assistance in the negative voltage sweeping processing. Meanwhile, the filled traps will discharge the electrons and the measurement current reduces quickly. The device resistance will maintains HRS until the majority traps have been emptied.

In order to discuss the device stability, the SET and RESET voltages distribution experiment was carried out under 100 sweep cycles, as shown in Fig. 4(a). It is obviously that the SET and RESET distribution voltages are ~0.4V and ~0.6V, respectively.

To further confirm the fabricated device potential in memory application, the cell retention characteristics were investigated under 0.3 V reading voltage at 85 °C for both resistance states and was shown in Fig. 4(b). It is clear that the both HRS and LRS resistance exhibit little change during th process, showing the nondestructive readout and nonvolatile nature characteristics. It is prove that the device is suitable for nonvolatile memory application.

a) *b)*
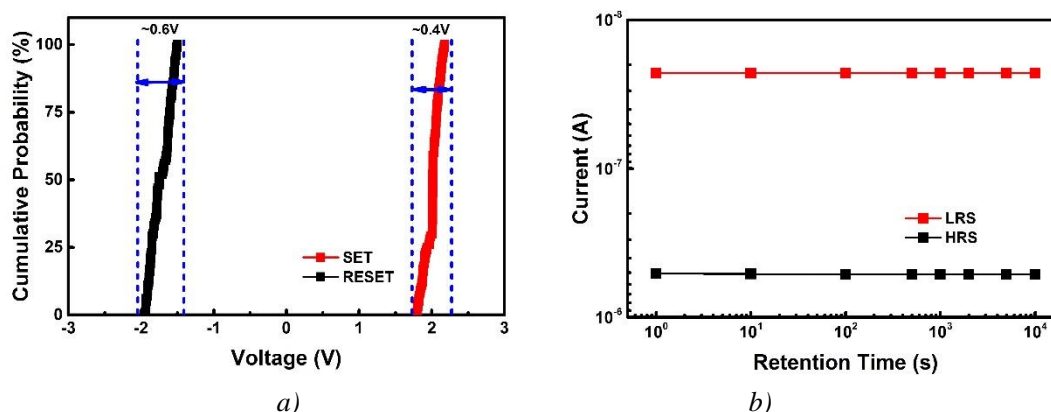
Fig. 4. (a). The probability plots of the SET and RESET voltage distributions for Ag /ZrO$_2$/Ta with 100 cycles. (b). The retention characteristics for Ag /ZrO$_2$/Ta.

4. Conclusions

In summary, the device of Ag/ZrO$_2$ /Ta was prepared by using the magnetron sputtering technique under room temperature. The device cross sectional SEM image shows clearly sandwich structure. The Raman spectra analysis reveals that the peak is related to the ZrO$_2$ phase. The sandwich structure device based on Ag/ZrO$_2$ /Ta shows stable bipolar RS characteristics and possess the excellent properties such as reversible switching, nondestructive readout, reproducible resistance, endurance cycling performance and nonvolatile storage. The fabricated device intrinsic RS mechanism is well interpreted by the Trap-limited space-charge limited conduction under the influence of the exponential trap distribution in the band gap. The SCLC model is contributed by the defects existing in the amorphous ZrO$_2$ film layer. Moreover, the RS based on amorphous ZrO$_2$ demonstrates as a promising material for nonvolatile memory application.

Acknowledgments

References

[1] L. O. Chua. IEEE Trans.Circuit Theory **18,** 5 (1971)
[2] Y. Yuan, X. Cao, Y. Sun, J. Su, C. Liu, L. Cheng, Y. Li, L. Yuan, H. Zhang and J. Li. Journal of Materials Science: Materials in Electronics **29,** 3 (2017)
[3] S. Ali, J. Bae, C. H. Lee, N. P. Kobayashi, S. Shin and A. Ali. Nanotechnology **29,** 45 (2018)
[4] Y. Li, X. Li, L. Fu, R. Chen, H. Wang and X. Gao. IEEE Transaction on electron device **65,**

12 (2018)

[5] J. J. Yang, D. B. Strukov and D. R. Stewart. Nature nanotechnology **8,** 1 (2013)

[6] M. Aljafar, P. Long and M. Perkowski. BioNanoScience **6,** 3 (2016)

[7] G. Du, Z. Chen, Q. Mao and Z. Ji. Applied Physics Letters **110,** 9 (2017)

[8] L. Fu, Y. Li, G. Han, X. Gao, C. Chen and P. Yuan. Microelectronic Engineering **172,** (2017)

[9] B. Sun, Y. X. Liu, L. F. Liu, N. Xu, Y. Wang, X. Y. Liu, R. Q. Han and J. F. Kang. Journal of Applied Physics **105,** 6 (2009)

[10] E. Linn, R. Rosezin, U. Bottger and R. Waser. Nanotechnology **23,** 30 (2012)

[11] M. J. Kim, K. R. Son, J. H. Park and T. G. Kim. Solid-State Electronics **132,** (2017)

[12] T. Shi, X. B. Yin, and X. Guo. Physical chemistry chemical physics : PCCP **18,** 14 (2016)

[13] Q. Zhang, H. Wu, P. Yao, W. Zhang, B. Gao, N. Deng and H. Qian. Neural networks : the official journal of the International Neural Network Society **108,** (2018)

[14] R. Islam, H. Li, P.-Y. Chen, W. Wan, H.-Y. Chen, B. Gao, H. Wu, S. Yu, K. Saraswat and H. S. Philip Wong. Journal of Physics D: Applied Physics **52,** 11 (2019)

[15] Young Jun Noh, Yoon-Jae Baek, C. J. K. Quanli Hu, Young Jin Choi, Hyun Ho Lee and T.-S. Yoon. IEEE TRANSACTIONS ON NANOTECHNOLOGY **14,** 5 (2015)

[16] X. Guo, F. Merrikh-Bayat, L. Gao, B. D. Hoskins, F. Alibart, B. Linares-Barranco, L. Theogarajan, C. Teuscher and D. B. Strukov. Frontiers in neuroscience **9,** (2015)

[17] W. Guan, S. Long, R. Jia and M. Liu. Applied Physics Letters **91,** 6 (2007)

[18] S. Stille, C. Lenser, R. Dittmann, A. Koehl, I. Krug, R. Muenstermann, J. Perlich, C. M. Schneider, U. Klemradt and R. Waser. Applied Physics Letters **100,** 22 (2012)

[19] Y. Li, Y. P. Zhong, J. J. Zhang, X. H. Xu, Q. Wang, L. Xu, H. J. Sun and X. S. Miao. Applied Physics Letters **103,** 4 (2013)

[20] Y. Yuan, X. Cao, Y. Sun, J. Su, C. Liu and J. Li. RSC Advances **7,** 73 (2017)

[21] D. Brunel, C. Anghel, D.-Y. Kim, S. Tahir, S. Lenfant, A. Filoramo, T. Kontos, D. Vuillaume, V. Jourdain and V. Derycke. Advanced Functional Materials **23,** 45 (2013)

[22] L. Li and D. Wen. Organic Electronics **34,** (2016)

[23] Y.-l. Jin, Z.-t. Xu, X. He, C. Wang and H.-b. Lu. Physica B: Condensed Matter **449,** (2014)

[24] C. Jia, J. Li, G. Yang, Y. Chen and W. Zhang. Nanoscale research letters **13,** 1 (2018)

[25] M. Park, S. Park and K. H. Yoo. ACS applied materials & interfaces **8,** 22 (2016)

[26] P. Parreira, S. McVitie and D. A. MacLaren. Journal of Physics D **49,** 9 (2016)

[27] W. Guan, M. Liu, S. Long, Q. Liu and W. Wang. Applied Physics Letters **93,** 22 (2008)

[28] Q. Liu, W. Guan, S. Long, R. Jia, M. Liu and J. Chen. Applied Physics Letters **92,** 1 (2008)

[29] Q. Zuo, Q. Liu, Y. Li, Y. Wang and M. Liu. Journal of Applied Physics **106,** 7 (2009)

[30] S. Long, Q. Liu, H. Lv, Y. Li and Y. Wang. Applied Physics A **102,** 4 (2011)

[31] F.-C. Chiu. Advances in Materials Science and Engineering **2014,** (2014)

[32] T.-L. Tsai, T.-H. Ho and T.-Y. Tseng. Journal of Physics D: Applied Physics **48,** 3 (2015)

[33] P. Rauwel, E. Rauwel, and A. Galeckas. Journal of Applied Physics **112,** 10 (2012)

[34] M. M. Yung, E. M. Holmgreen and U. S. Ozkan. Catalysis Letters **118,** 3-4 (2007)

[35] F. C. Chiu. Advances in Materials Science and Engineering **2014,** (2014)

[36] Y.-M. Koo, S.-J. Choi, T.-Y. Chu and T.-H. Yoon. Journal of Applied Physics **104,** 12 (2008)

[37] D. S. Shang, Q. Wang, L. D. Chen, and W. Q. Zhang. Physical Review B **73,** 24 (2006)